

1

2 ENERGY CORRELATORS AS A PROBE OF THE HARD PROCESS IN RUN 24  $p - p$   
3 COLLISIONS AT  $\sqrt{s} = 200 \text{ GeV}$  WITH THE sPHENIX DETECTOR AT RHIC

4 by

5 SKADI KURT GROSSBERNDT

6 A dissertation submitted to the Graduate Faculty in Physics in partial fulfillment of the  
7 requirements for the degree of Doctor of Philosophy, The City University of New York

8 2025

9

10

© 2025

11

SKADI KURT GROSSBERNDT

12

All Rights Reserved

- <sup>13</sup> This manuscript has been read and accepted by the Graduate Faculty in Physics in  
<sup>14</sup> satisfaction of the dissertation requirement for the degree of Doctor of Philosophy.

**Professor Stefan Bathe**

---

Date Chair of Examining Committee

15

**Professor Daniel Kabat**

---

Date Executive Officer

**Professor Adrian Dimitru**

**Professor Raghav Kunnawalkam Elayavalli**

16

**Professor Jamal Jallian-Marian**

**Professor Miguel Castro Nunes Fiolhais**

Supervisory Committee

17

### Abstract

ENERGY CORRELATORS AS A PROBE OF THE HARD PROCESS IN RUN 24  $p - p$

## COLLISIONS AT $\sqrt{s} = 200$ GeV WITH THE SPHENIX DETECTOR AT RHIC

by

SKADI K GROSSBERNDT

<sup>23</sup> Adviser: Professor Stefan Bathe

<sup>24</sup> This dissertation consists of three parts in addition to a literature review establishing the  
<sup>25</sup> state of the art of jet physics and the Energy-Energy correlator at high energies...

**26 Part 1: Hardware** This part discusses the physical hardware used to make the measure-  
27 ments of the energy in the jets created by the proton-proton collisions. This part contains a  
28 discussion of the sPHENIX detector and an in-depth look at the relevant susbsystems for the  
29 meausements in this analysis. In addition, the Monte Carlo methods and models to discern  
30 the expected respnse and calibrate the detector are discussed in detail, with both subparts  
31 coming together in a disucssion of backgrounds and error calculation in general and for the  
32 observables at hand.

<sup>33</sup> **Part 2: Technicalities** This part builds from first principles up to the jet measurement  
<sup>34</sup> in a theoretical light, and then discusses the additional computational techniques on display  
<sup>35</sup> that will provide the bridge between the theory of these observables and the practical ap-  
<sup>36</sup> plication to sPHENIX. This part contains a chapter that is a pared down discussion of a  
<sup>37</sup> midstream paper proposed as part of the thesis process that establishes the safety of this  
<sup>38</sup> observable against jet finding choices.

<sup>39</sup> **Part 3: Experimental Output** This part is the meat and potatoes of the dissertation,  
<sup>40</sup> discussing results from the experiment and the analysis in light of the previous parts and  
<sup>41</sup> comparing to the world results from related systems.

# <sup>42</sup> Contents

<sup>43</sup> <b>1 Literature Review</b>	<sup>1</sup>
44     1.1 Jets Definitions . . . . .	2
45         1.1.1 Jet Reconstruction Algorithms . . . . .	2
46         1.1.2 Quark and Gluon Jets . . . . .	5
47     1.2 Jet Substructure Measurements . . . . .	5
48     1.3 N-Point Energy Correlator . . . . .	5
<sup>49</sup> <b>I Hardware: The Detector and Simulations</b>	<sup>6</sup>
<sup>50</sup> <b>2 The sPHENIX detector</b>	<sup>7</sup>
51     2.1 Calorimetry . . . . .	8
52         2.1.1 Analog Digital Converters and Data Acquisition . . . . .	8
53         2.1.2 Hadronic Calorimeters . . . . .	10
54         2.1.3 Electromagnetic Calorimeter . . . . .	12
55         2.1.4 Zero Degree Calorimeter . . . . .	12
56     2.2 Tracking . . . . .	13
57         2.2.1 TPC Outer Tracker . . . . .	13
58         2.2.2 Time Projection Chamber . . . . .	14
59         2.2.3 Intermediate Silicon Tracking Detector . . . . .	14

CONTENTS	vii
60        2.2.4    Micromegas Vertex Detector . . . . .	14
61        2.2.5    Event Reconstruction and Track Matching . . . . .	14
62        2.3      Event Characterization . . . . .	14
63        2.3.1    sPhenix Event Plane Detector . . . . .	14
64        2.3.2    Minimum Bias Detector . . . . .	14
65        2.4      Triggers . . . . .	14
66        2.4.1    Jet Triggers . . . . .	15
67        2.4.2    Photon Triggers . . . . .	15
68        2.4.3    Minimum Bias Trigger . . . . .	15
69 <b>3 Monte Carlo Simulations</b>	16
70 <b>4 Determining Backgrounds and Errors</b>	17
71 <b>II Technicalities: The finer points of theory and computing</b>	18
72 <b>5 The Energy Correlator and the primary vertex</b>	19
73 <b>6 Jets in Vacuum and the PDF</b>	20
74        6.1      Jet Identification Algorithms . . . . .	20
75 <b>7 So exactly how intelligent is AI</b>	21
76 <b>8 Proof Solving and Validation as Quality Control Mechanisms</b>	22
77 <b>III Experimental Output: The Main Event</b>	23
78 <b>9 So is sPHENIX actually working?</b>	24

<i>CONTENTS</i>	viii
<b>79 10 Measuring the Energy Correlator</b>	<b>25</b>
80    10.1 Discretization and Efficiency . . . . .	25
81    10.2 Whole Calorimeter Measurements . . . . .	26
<b>82 11 The Power of the ENC: <math>\alpha_s</math> at the few GeV scale</b>	<b>28</b>
<b>83 12 Event-by-Event distinguishing</b>	<b>29</b>
<b>84 13 Comparison is the Theft of Joy: What does the LHC say, and how about</b>	
85 <b>STAR?</b>	<b>30</b>
<b>86 14 Entanglement and other Lofty Goals</b>	<b>31</b>
<b>87 IV Wrapping it all up</b>	<b>32</b>
<b>88 15 Observable prospects for Run 25 and the EIC</b>	<b>33</b>
<b>89 16 Remaining Questions</b>	<b>34</b>
<b>90 17 Implementation and application for the remaining sPHENIX data</b>	<b>35</b>

<sup>91</sup> **List of Tables**

## <sup>92</sup> List of Figures

<sup>93</sup>	2.1 The sPHENIX detector. The Zero Degree Calorimeter is not picutred but is located further along the beam pipe. . . . .	8
<sup>94</sup>		
<sup>95</sup>	2.2 Top: Persistence Waveform. Bottom: Energy distribution averaged across	
<sup>96</sup>	$10^5$ events . . . . .	11
<sup>97</sup>		
<sup>98</sup>	10.1 Multiplicity in each Calorimeter (pending–have ohcal now) as percentage of towers with $E \geq 10$ MeV to filter out electronics fluctuations . . . . .	27

<sup>99</sup> Chapter 1

<sup>100</sup> Literature Review

## **1.1 Jets Definitions**

The study of Quantum Chromodynamics in high energy collisions, such as those at the Relativistic Heavy Ion Collider or the Large Hadron Collider, is often carried out through investigation of the kinematics of jets. Jets, as objects, sit in the boundary between experiment and theory, being an experimental signature corresponding to final states of quarks and gluons produced in collisions. Jets are a cluster of final state particles that result from the showering and hadronization of the initial parton, that are identified in experiment through use of one of the multiple jet reconstruction algorithms.

### **1.1.1 Jet Reconstruction Algorithms**

In Ryan Atkin's paper *Review of jet reconstruction algorithms* [1], Atkin provides an overview of the standard algorithms with a focus on practical implementation for experimental usage. Atkin discusses a number of algorithms that fall into two categories: Cone based and Sequential Clustering

#### **114 Cone Methods**

In Atkin's paper, Atkin discusses two iterative cone procedures—Iterative Cone with Progressive Removal (IC-PR) and with Split Merge (IC-SM)—and one more modern cone method, Seedless Infrared Safe Cone (SIS-Cone). These iterative cone procedures are described as simple to implement in an experimental context, however, they both suffer deficiencies from a theoretical perspective as they fail to be IRC safe [1] [2]. In principle, these clustering algorithms are rather similar, one takes the hardest particle in the final state, terms this a jet seed and draws a circle of a fixed size around it, summing the 4-momentum of all particles of within the circle. Then, the jet axis is compared to the jet seed, where a properly identified

123 cone is defined as one where the condition in eq (1.1) is fulfilled.

$$\frac{p_{\text{jet}}^{\mu}}{|p_{\text{jet}}|} = \frac{p_{\text{seed}}^{\mu}}{|p_{\text{seed}}|} \quad (1.1)$$

124 If this condition is not fulfilled, one then starts again, setting the seed at the axis of the  
125 previously identified cone and draws a new circle of the same radius centered there. Once  
126 the jet is identified, the progressive removal procedure then removes all particles identified  
127 with this method and continues until there are no particles with a  $p_T > p_T^{min}$  which is set by  
128 the user. In the split-merge procedure, one first identifies all seed particles, and builds the  
129 stable cones, but these are then treated as protojets. These protojets are then filtered by an  
130 additional  $p_T^{\text{jet}} > p_T^{\text{cut}}$  threshold, then overlapping protojets are split or merged in descending  
131  $p_T$  order depending on a merging parameter,  $f \approx 0.5$ . If the sum of  $p_T$  for the shared particles  
132 is less than the  $fp_T^{sl}$  where  $p_T^{sl}$  is the lower  $p_T$  protojet, then the overlapping particles are  
133 split based on distance from the protojet axes and the protojets are updated. Else wise, the  
134 two protojets are merged into a single jet.

135 Both of these methods are IRC unsafe to some degree, but are useful in situations where  
136 quick jet identification is needed, e.g. CMS Cone and Pythia Cone are IC-PR and ATLAS  
137 Cone and JetClu midpoint cones are IC-SM. The IC-PR is collinear unsafe, as the progressive  
138 removal procedure inherently ignores any overlapping jets. The IC-SM however is infrared-  
139 unsafe as it introduces further parameters to filter pile-up and thus removes low energy  
140 contributions [2].

## 141 Sequential Clustering algorithms

142 The sequential clustering algorithms on the other hand are all IRC safe, working from the  
143 underlying assumption that all of the final state particles in a jet would have originated from  
144 a single initial parton, thus in theory, one can reconstruct that collection [3]. Three of these

<sub>145</sub> methods, anti- $k_T$ ,  $k_T$  and Cambridge/Achen, utilize the same mechanism with modifications  
<sub>146</sub> to their metric. These methods, here referred to as  $k_T$ -type, rely on the evaluation of a  
<sub>147</sub> distance metric of the form,

$$d_{ij} = \min \{p_{T,i}^{2n}, p_{T,j}^{2n}\} \frac{\Delta R_{ij}}{R} \quad d_i = p_{T,i}^{2n} \quad (1.2)$$

<sub>148</sub> Where  $n = 1$  is  $k_T$ ,  $n = 0$  is the Cambridge/Achen and  $n = -1$  is the anti- $k_T$ ,  $\Delta R_{ij}$  is  
<sub>149</sub> the angular distance between the jets in  $\phi - y(\eta)$  space and  $R$  is the size of the jet, which  
<sub>150</sub> functions as an estimated value of the average jet radius, a parameter set by the analyzer.  
<sub>151</sub> One clusters particles together by finding  $\min \{\{d_{ij}\}, \{d_i\}\}$  and, if the minimum value is one  
<sub>152</sub> of these  $d_{ij}$  then one clusters those two, adds their 4 momentum together and recalculates the  
<sub>153</sub> distance metric. If the minimum is a  $d_i$ -called beam distance, then the protojet is promoted  
<sub>154</sub> to a jet and then removed from the set of candidates. While these methods are IRC safe [3],  
<sub>155</sub> they do suffer from a similar tuning problem as the cone methods, where misidentification of  
<sub>156</sub> jets is possible depending on the  $R$  value and  $p_T$  cutoff, however, both of these parameters  
<sub>157</sub> can be estimated well and have led to a standard prescription of the anti- $k_T$  method at a  
<sub>158</sub> variety of  $R$ , usually prioritizing the  $R = 0.4$  jet as the best balance between exclusion and  
<sub>159</sub> false positive jet particles. Of note for the analysis of this system, the  $k_T$ -type algorithms  
<sub>160</sub> can produce different collections of jet particles and different shapes of the final state of the  
<sub>161</sub> jet. The anti- $k_T$  method produces circular cones as a function of its metric, thus making it  
<sub>162</sub> more directly comparable to the previous cone methods, while the  $k_T$  method will produce  
<sub>163</sub> final states of various sizes. This discrepancy proves useful in analysis of jet substructure  
<sub>164</sub> observables, such as the primary family of observables, the Energy-Energy Correlators, in  
<sub>165</sub> this thesis, as it allows for a lund Plane analysis of the jet structure that combines anti- $k_T$   
<sub>166</sub> and  $k_T$  techniques to improve veracity of the analysis method

### **1.1.2 Quark and Gluon Jets**

In their paper *An Operational Definition of Quark and Gluon Jets* [4] Kimiske, Metodiev and Thaler present a theoretical definition of jet flavor with an eye towards application at colliders. They aim to present a precise and practical definition of jet flavor at the hadron level, thus allowing for direct measurement from collider experiments rather than a measurement by proxy. While the gluon or quark jet is well defined at the level of the hard scattering, corresponding to an initiating parton of the primary vertex [5] [6]. Experimentally, there is significant interest in being able to discriminate quark and gluon jets in searches for Beyond Standard Model physics, searches for Dark Matter, in jet substructure analysis and in QGP physics. [7][8][9][10]. The determination of relative populations of quark and gluon jets in a dijet sample is one of the primary tasks of this thesis and will be discussed at length in chapters 11 and 12.

Kimiske et al.-from here referred to as KMT-set their work in the context of discerning

the quark-gluon jet populations in samples rather than applying an event-by-event labeling scheme. KMT's work begins with the consideration of two samples of data with jets at a fixed  $p_T$  range with the condition that one be gluon enriched and one quark enriched. In the specific test case presented in KMT, a Z-jet sample (gluon enriched) and a  $\gamma$ -jet sample (quark-enriched) are used.

## **1.2 Jet Substructure Measurements**

## **1.3 N-Point Energy Correlator**

187

## Part I

188

### Hardware: The Detector and Simulations

189

<sub>190</sub> **Chapter 2**

<sub>191</sub> **The sPHENIX detector**

<sub>192</sub> The sPHENIX detector is part of the Relativistic Heavy Ion Collider (RHIC) complex at  
<sub>193</sub> Brookhaven National Laboratories (BNL) in Upton, New York. RHIC is one of two major  
<sub>194</sub> circular particle colliders in the world, the other of which is the Large Hadron Collider at  
<sub>195</sub> CERN in Geneva, Switzerland. Over the course of the sPHENIX experiment which will run  
<sub>196</sub> from run 23 until RHIC ceases operations after run 25, RHIC will be colliding gold nuclei  
<sub>197</sub> and protons with run 23 having been dedicated to commissioning Au+Au running, run 24  
<sub>198</sub> dedicated to p+p with three weeks of Au+Au for further tracking commissioning and run  
<sub>199</sub> 25 dedicated to physics running in Au+Au collisions. RHIC runs with a center of mass  
<sub>200</sub> energy of  $\sqrt{s} = 200\text{GeV}$  for both protons and gold, and additionally is the sole collider  
<sub>201</sub> that collides polarized protons, which allows for more in depth studies of spin physics. At  
<sub>202</sub> RHIC, sPHENIX's forerunner, the Pioneering High Energy Nuclear Interaction eXperiment  
<sub>203</sub> (PHENIX), performed the first measurement of the Quark Gluon Plasma droplets [10] in  
<sub>204</sub> nuclei-nuclei collisions.

<sub>205</sub> sPHENIX is designed to offer significant upgrades to PHENIX, specifically providing in-  
<sub>206</sub> creased coverage with hadronic and electromagnetic calorimeters, increasing effectiveness in  
<sub>207</sub> studies of jets and heavy flavor at mid-to-high Bjorken x [11][12][13] Broadly, sPHENIX can

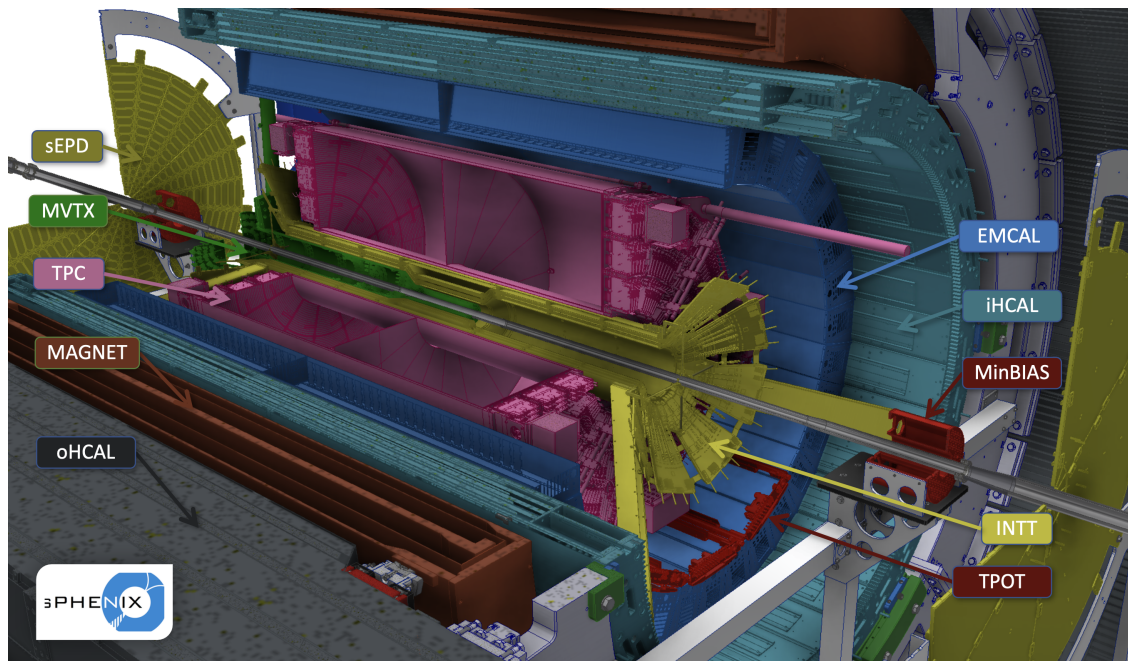


Figure 2.1: The sPHENIX detector. The Zero Degree Calorimeter is not pictured but is located further along the beam pipe.

208 be broken into three categories of subsystem: Calorimeters, Tracking and Event characteri-  
209 zation.

210 sPHENIX is constructed around a 1.5 Tesla superconducting magnet, cooled by liquid  
211 helium, which was previously used on the BABAR experiment at SLAC, with the outer  
212 hadronic calorimeter sitting on the outer radius of the magnet, as seen in fig 2.1

## 213 2.1 Calorimetry

### 214 2.1.1 Analog Digital Converters and Data Acquisition

215 Beyond the purposes and hardware of the detector itself, one can further characterize the  
216 subsystems of sPHENIX into streaming readout and non-streaming detectors, broadly dis-  
217 tinguishing the tracking detectors from other subsystems. The non-streaming detectors all  
218 use a common data acquisition pipeline and data format. These detectors are readout to

analog digital converters boards with 64 channels each, which are then grouped into sets of 3 called an "XMIT" group, which is then read to the data format as a "packet" of 192 channels. Each packet is transmitted from the detector to the computing center on a separate fiber optic cable that is then read into a digitizer which forms groups of (at most) eight packets that are then assigned to individual data acquisition servers. The digitizing process allows for readback into the detector through a global trigger and timing module, where each DAQ server, can issue commands and readback to an event building logic that will then flow back to the detector controlling the same XMIT groups. Each set of (at most) 4 XMIT groups is arranged into a crate with a single crate controller that receives trigger and timing information distributed via a global timing and level 1 trigger module (GL1/GTM) that is then processed through a clockmaster for each digitizer rack, which will hold between 1 and 4 crates, depending of the needs of the subsystem. The data read out to each DAQ server is then stored in the "Porschke Raq Data Format" or prdf file that provides an event structure consisting of a header with some identifying information and separate headers for each packet, but is otherwise comprehensible as an ASCII file. This event structure allows for easy offline combination of events across the calorimeters while keeping individual file size buffers relatively small, as each packet has timing information along with an event number relative to the run that is inherited from the timing module. This DAQ configuration is currently used for the calorimeters, the event plane detector and the minimum bias detector, which allows for faster event building to verify data quality and alignment. The tracking detectors utilize a streaming readout format that creates event pools that are then associated with beam crossing timings provided by the RHIC clock and can be matched onto the GTM timing in offline analysis. This process is slow, and the full implementation of event combination is still under development, not accounting for event reconstructions which involves track matching across subsystems and will be discussed in section 2.2.5.

<sup>244</sup> **ADC Zero Suppression**

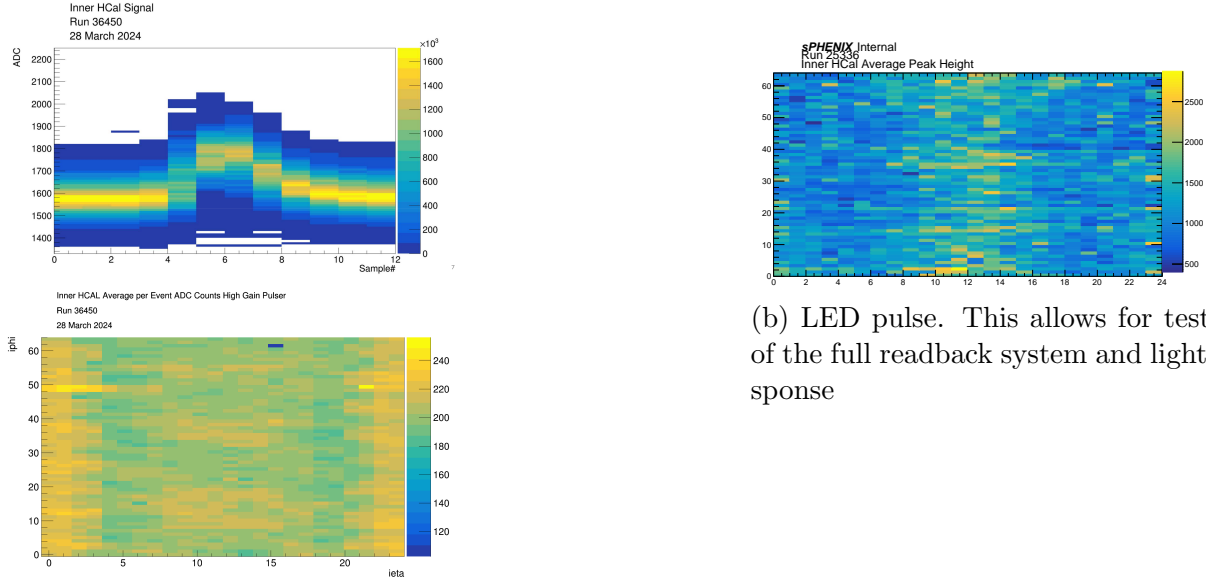
<sup>245</sup> While this system allows for a simplified readout of the calorimetry system, one expects  
<sup>246</sup> that, for the average event, most of the towers will be dominated by noise, thus one wastes  
<sup>247</sup> significant computational resources on reading and storing data that will be immediately  
<sup>248</sup> discarded. This decreases readout rates, runs the risk of filling the storage systems and  
<sup>249</sup> increases the likelihood of register errors that require restarting runs; in summary, these  
<sup>250</sup> null data points give no useful physics and hurt our ability to consistently take data. The  
<sup>251</sup> ADC and readout electronic systems are thus equipped with a zero suppression system that  
<sup>252</sup> allows for onboard discrimination and data reduction. At the FPGA level, each channel  
<sup>253</sup> is individually evaluated by taking a post-pre measurement and comparing to a threshold  
<sup>254</sup> derived from studies of average noise in each channel

$$ADC_{\text{sample } 6} - ADC_{\text{sample } 0} > E_{\text{cut off}} \quad (2.1)$$

<sup>255</sup> Where the evaluation shown in eq (2.1) assumes that the ADC readout has been properly  
<sup>256</sup> timed in relative to the trigger such that the peak of well formed data should be centered  
<sup>257</sup> near sample 6 (of 12, 16 or 31), and one can take a cutoff with resolution as wide as a  
<sup>258</sup> single number and as granular as a tower-by-tower volume. Studies have been performed at  
<sup>259</sup> sPHENIX to establish good thresholds for this zero-suppression approach and validate that  
<sup>260</sup> this will not introduce biasing into the detector [14].

<sup>261</sup> **2.1.2 Hadronic Calorimeters**

<sup>262</sup> sPHENIX's power in jet physics comes in large part from its calorimeter systems, including  
<sup>263</sup> two separate hadronic calorimeters. The outer and inner hadronic calorimeter (OHCAL and  
<sup>264</sup> IHCal respectively) are both divided into 24 bins in  $\eta$  with coverage of  $|\eta| \leq 1.1$  and full  
<sup>265</sup>  $\varphi$  coverage with 64 bins in  $\varphi$ , grouped in  $\varphi$  into 32 sectors in each calorimeter. Each



(a) Charge Injection Pulse. This system allows for direct testing of electronics without detector response

Figure 2.2: Top: Presistence Waveform. Bottom: Energy distribution averaged across  $10^5$  events

hadronic calorimeter therefore has tower size of  $\delta\eta = 0.092$  and  $\delta\varphi = 0.098$ . The outer hadronic calorimeter is constructed of steel and sits outside of the magnet, with inner radius of  $r = 1.82$  m and outer radius of  $r = 2.69$  m. The inner hadronic calorimeter is constructed of aluminum and sits just inside the magnet, with inner radius of  $r = 1/16$  m and outer radius of  $r = 1.37$  m. Each tower corresponds to a readout board that sums readout from four scintillator paddles embeded into the calorimeter as show in fig. ???. These interface boards form a single readout channel, and can be individually teste via a pulser system that injects charge into the interface board testing readback independent of scintillator response, and LED system that injects a fixed pulse of light into the scintillators to test behavior of the Silicon Photomultipliers (SiPMs). Output of each of these systems is shown in fig 2.2

**276 Calibration**

277 The hadronic calorimeters were intially calibrated through use of cosmic ray muons, matching  
278 the spectra to Monte Carlo generated through EcoMug and GEANT4 [**HCal'Calib**]. This  
279 calibration is updated throughout the run via continued cosmic ray studies in between physics  
280 data taking, in addition to ongoing work on in-situ calibrations using tower-slope methods  
281 [**tower'slope'hcal**]. These calibrations have yeilded an average conversion factor for the  
282 OHCal of and the IHCal of

**283 2.1.3 Electromagnetic Calorimeter**

284 Moving in one layer from the hadronic calorimeter, the Electromagnetic Calorimeter (EM-  
285 Cal) has the same coverage in  $\eta - \varphi$  space, but has 16 times as many towers with 96 bins in  
286  $\eta$  and 256 bins in  $\varphi$ . The EMCAL is constructed of blocks of tungsten with embedded scin-  
287 tilationg fibers, and had inner radius  $r = 0.9$  m and outer radius of  $r = 1.16$  m. Similarly  
288 to the HCals, the EMCAL is also equipped with a pulser and LED, although the increased  
289 number of towers and higher varaiblility in response requires that different pulse widths be  
290 used for seperate sets of towers to prevent saturation and clipping on the LED pulse.

**291 Calibration**

292 The EMCAL was calibrated to the  $\pi^0$  mass through the  $\pi^0 \rightarrow \gamma\gamma$  decay channel with additional  
293 corrections applied via the tower slope. The mean  $m_{\pi^0}$  and width are used as quality  
294 assurance plots to monitor radiation damage to the EMCAL on an ongoing basis.

**295 2.1.4 Zero Degree Calorimeter**

296 The Zero Degree Calorimeter (ZDC) is a small transverse energy hadron detector that po-  
297 sitioned outside of the experiment hall, in the tunnels along the beam pipe, 18 m from the

298 interaction point on both side. The ZDC is used to detect spectator neutrons to allow for the  
299 calculation of multiplicity and event geometry, making it an overlapping detector between  
300 the calorimeters and the event characterization [15]. In addition, the ZDC provides a good  
301 proxy for total collision rates, useful for both real time monitoring of beam conditions and  
302 The sPHENIX ZDC is one of two detectors that was preserved from PHENIX, with minor  
303 repairs and upgrades to improve running. In pp collisions, the ZDC provides additional  
304 utility as a spin momentum detector that allows for measurement of the spin patterns of the  
305 RHIC beam through the Vernier Scan. This functionality is pivotal for the development  
306 of sPHENIX's spin physics program in pp and its extensions into the continuing physics  
307 goals at the Electron Ion Collider (EIC)[15]. For the purposes of this work, the ZDC is not  
308 utilized for either spin physics or trigger capabilities and serves primarily to help establish  
309 cross-sections for error determination. While this work does not dive into the subject of  
310 spin dependence, such topics are a natural extension and present an interesting avenue for  
311 future studies in this vein to be done with the sPHENIX Run 24 data set.

## 312 **2.2 Tracking**

313 The sPHENIX tracking system consists of the Silicon tracking and vertexing detectors and  
314 the gas based trackers. These systems are designed for fast readout, precise momentum  
315 resolution and secondary vertex detection

### 316 **2.2.1 TPC Outer Tracker**

317 The TPC Outer Tracker (TPOT) was designed as a minimal add-on to improve tracking  
318 efficiency and resolution by providing additional track points.

### **319 2.2.2 Time Projection Chamber**

320 The Time Projection Chamber (TPC) is a gas based detector designed to track

### **321 2.2.3 Intermediate Silicon Tracking Detector**

322 The INTermediate Silicon Tracking detector (INTT) consists of two layers of semiconducting  
323 silicon

### **324 2.2.4 Micromegas Vertex Detector**

325 The Micromegas Vertex detector (MVTX) is a silicon based vertexing detector based on a  
326 similar system at the ALICE experiment of the Large Hadron Collider (LHC).

### **327 2.2.5 Event Reconstruction and Track Matching**

## **328 2.3 Event Characterization**

### **329 2.3.1 sPhenix Event Plane Detector**

### **330 2.3.2 Minimum Bias Detector**

331 The sPHENIX Minimum Bias Detector (MBD) is the other detector preserved from PHENIX,  
332 when it was called the Beam-Beam Counter (BBC). This detector is situated

## **333 2.4 Triggers**

334 The sPHENIX detector has a number of triggers at its disposal to allow for online event  
335 type selections for the triggered readout system: the EMCal, the HCals, the ZDC, the  
336 MBD, the sEPD and—for run 2024—the TPC. Starting in run 2024, available triggers are

<sup>337</sup> ZDC and Minimum Bias in single and coincidence modes, a restricted vertex Minimum Bias  
<sup>338</sup> trigger, four jet triggers at differing minimum energy thresholds (6-12 GeV with variation  
<sup>339</sup> through the run), four photon triggers at differing minimum energy thresholds (2-10 GeV  
<sup>340</sup> with variation through out the run), random triggers, clock triggers and jet with Minimum  
<sup>341</sup> Bias triggers. In order to decrease busy signals, the overall trigger rate is scaled down to 8  
<sup>342</sup> kHz, taking 100 Hz of clock triggers as a control, full rate rare event (jet and photon) and  
<sup>343</sup> minmum bias filling the remaining.

<sup>344</sup> **2.4.1 Jet Triggers**

<sup>345</sup> **2.4.2 Photon Triggers**

<sup>346</sup> **2.4.3 Minimum Bias Trigger**

<sup>347</sup>

# Chapter 3

<sup>348</sup>

## Monte Carlo Simulations

<sup>349</sup> For proton-proton collisions, sPHENIX has  $10^8$  fully reconstructed events from Pythia 8  
<sup>350</sup> and Herwig 7 for  $2 \rightarrow 2$  and minimum bias (soft QCD) events that are then reconstructed  
<sup>351</sup> using GEANT. While there is a jet sample that has been performed with the detroit tune  
<sup>352</sup> [**Detroit**·**tune**] and there is an existing, equivalent tune for Herwig [**New**·**Haven**·**Vanderbilt**·**tune**],  
<sup>353</sup> in this work, I focus on the default tuned sample as there is a wider dataset from which to  
<sup>354</sup> draw. data from the 2 and three point energy correlator, and its important for training of  
<sup>355</sup> our discriminator

<sup>356</sup> Chapter 4

<sup>357</sup> Determining Backgrounds and Errors

358

## Part II

359

**Technicalities: The finer points of  
theory and computing**

360

<sup>361</sup> **Chapter 5**

<sup>362</sup> **The Energy Correlator and the**

<sup>363</sup> **primary vertex**

<sup>364</sup> Considering the limitations of Calorimetry only measuremet with RHIC one is So the energy  
<sup>365</sup> correlator allows a look back, I guess thaths the relevant bit? Point being, if the jet points  
<sup>366</sup> back to the primary vertex, the share of the energy between the jets and the composition of  
<sup>367</sup> those jets is directly determined by the  $2 \rightarrow 2$  scattering and is thus sensitive to the parton  
<sup>368</sup> distribution functions of the beam particles. Starting from the definition of the energy  
<sup>369</sup> correlator given in [16]:

$$\mathcal{E}_N = \int \frac{d\Omega}{2} \int d\vec{n}_{12} \frac{\langle \varepsilon(\vec{n}_1) \dots \varepsilon(\vec{n}_2) \rangle}{Q^2} \delta(\vec{n}_1 \cdot \vec{n}_2 - 2|\vec{n}_1| |\vec{n}_2| \cos \theta) \quad (5.1)$$

<sup>370</sup> Where  $\varepsilon(\vec{n}_i)$  is the energy flow operator defined as

$$\varepsilon(\vec{n}_i) = \lim_{r \rightarrow \infty} r^2 \int_{-\infty}^{\infty} dt \vec{n}^i T_i^0(t, r\vec{n}) \quad (5.2)$$

## **5.1 The primary vertex and interaction**

The goal of this work is to extract gluon distributions from the jet, thus one must consider those initial vertices that (to first order) produce the gluon-quark, gluon-gluon, and quark-quark dijet events. To this end, one considers the following tree level diagrams. While the processes are not immediately apparent in the final state of the jet, one notes that the two and three point energy correlators give a useful distinction as the jet function can be divided out, leaving a vertex dependent term at  $R_L \approx 2R_{\text{jet}}$

<sup>378</sup> **Chapter 6**

<sup>379</sup> **Jets in Vacuum and the PDF**

<sup>380</sup> **6.1 Jet Identification Algorithms**

<sup>381</sup> As discussed in chapter 1, there are a variety of jet finding algorithms that prioritize different  
<sup>382</sup> theoretical aspects of the underlying physics while being experimentally realizable [3] [1].

<sup>383</sup> In general, a jet identification algorithm needs to be IRC safe. That is, the jet object  
<sup>384</sup> needs to display invariance in the Infrared (IR) and Collinear regimes, managing real-virtual  
<sup>385</sup> cancellation and keeping results meaningful for emission and splitting respectively.

<sup>386</sup> Chapter 7

<sup>387</sup> So exactly how intelligent is AI

<sup>388</sup> Chapter 8

<sup>389</sup> Proof Solving and Validation as  
<sup>390</sup> Quality Control Mechanisms

391

## Part III

392

# Experimental Output: The Main Event

393

<sup>394</sup> Chapter 9

<sup>395</sup> So is sPHENIX actually working?

<sup>396</sup> **Chapter 10**

<sup>397</sup> **Measuring the Energy Correlator**

<sup>398</sup> **10.1 Discretization and Efficiency**

<sup>399</sup> In the discussion of the energy correlator in chapter 5, we had been working in an idealized  
<sup>400</sup> regime where the measurement is able to be resolved to arbitrary size, however, this is limited  
<sup>401</sup> by the physical reality of the detector systems.

<sup>402</sup> Even in simulations, one finds that the practical reality of making measurements of  
<sup>403</sup> the Energy correlator is severely hamstrung by the use of tower size objects rather than  
<sup>404</sup> the truth particles that make up our idealized toy jets discussed in section 6.1. To study  
<sup>405</sup> the efficiency loss, one takes the identified truth jet objects from Monte Carlo Simulations  
<sup>406</sup> (Pythia8 and Herwig for pp; sHIJING, EPOS4, AMPT for AuAu) and runs them through  
<sup>407</sup> Geant simulations to model detector effects. One then takes the initial truth jet, draws  
<sup>408</sup> a circle that encloses the truth particles, and projects this out onto the calibrated tower  
<sup>409</sup> response in each calorimeter, as well as runs an anti- $k_T$  jet identification algorithm to simulate  
<sup>410</sup> jet reconstruction. These three object types (truth jet, projective cone and reconstructed jet)  
<sup>411</sup> are collected into sets and the measurement of the two- and three-point energy correlators

<sup>412</sup> is performed using the defintion in eq 10.1

$$\langle E2C(R_L) \rangle = \frac{1}{N_{\text{events}}} \sum_{\text{events}} \frac{1}{N_{\text{jet}}} \sum_{N_{\text{jets}}} \sum_{i,j \in \text{Jet Constituents}} \frac{E_i E_j}{E_{\text{jets}}^2} \delta(R_{ij} - R_L) \quad (10.1)$$

$$\langle E3C(R_L) \rangle = \frac{1}{N_{\text{events}}} \sum_{\text{events}} \frac{1}{N_{\text{jet}}} \sum_{N_{\text{jets}}} \sum_{i,j,k \in \text{Jet Constituents}} \frac{E_i E_j E_k}{E_{\text{jets}}^3} \delta(\max R_{i,j,k} - R_L)$$

## <sup>413</sup> 10.2 Whole Calorimeter Measurements

<sup>414</sup> While the Energy correlator is generally studied within a jet, one can make use of the whole  
<sup>415</sup> calorimeter to compare the energy correlator across all angular seperations to characterize  
<sup>416</sup> the underlying event. This induces a new computational issue of scale, where the number  
<sup>417</sup> of calculations goes from  ${}_{50}C_2 = 1225$  in the HCAL and  ${}_{804}C_2 = 322,806$  in the EMCAL  
<sup>418</sup> to  ${}_{1536}C_2 \approx 2.4 \times 10^6$  and  ${}_{24576}C_2 \approx 6 \times 10^8$  in the EMCAL. However, since pp events  
<sup>419</sup> have relatively low multiplicity in the calorimeters as is seen in fig 10.1, one reduces the  
<sup>420</sup> computational load signifigantly by preprocessing the towers to remove all towers with energy  
<sup>421</sup> below some threshold, functionally mirroring the zero-suppression procedure discussed in  
<sup>422</sup> section 2.1.1. While

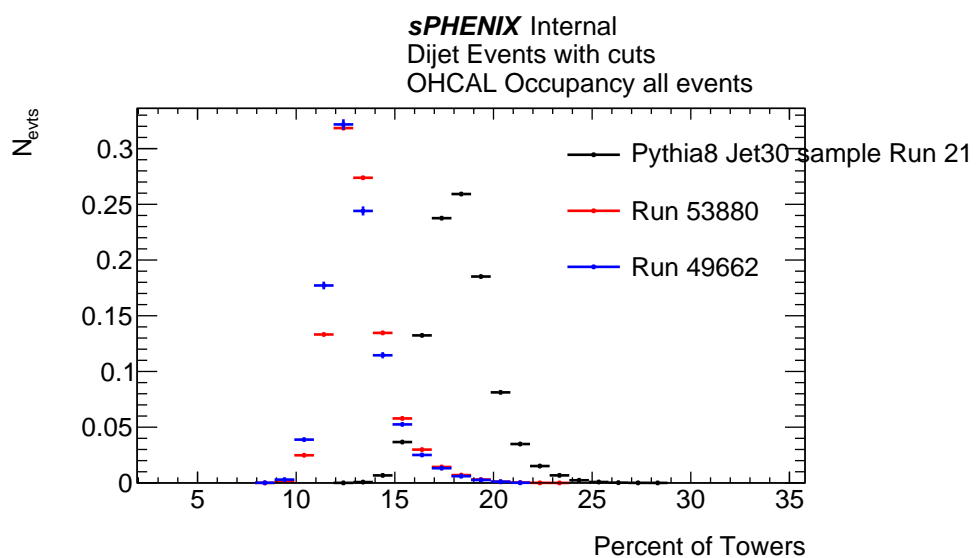


Figure 10.1: Multiplicity in each Calorimeter (pending—have ohcal now) as percentage of towers with  $E \geq 10$  MeV to filter out electronics fluctuations

<sub>423</sub> Chapter 11

<sub>424</sub> The Power of the ENC:  $\alpha_s$  at the few  
<sub>425</sub> GeV scale

<sup>426</sup> Chapter 12

<sup>427</sup> Event-by-Event distinguishing

<sup>428</sup> Chapter 13

<sup>429</sup> Comparison is the Theft of Joy: What  
<sup>430</sup> does the LHC say, and how about  
<sup>431</sup> STAR?

<sup>432</sup> Chapter 14

<sup>433</sup> Entanglement and other Lofty Goals

434

## Part IV

435

Wrapping it all up

<sup>436</sup> Chapter 15

<sup>437</sup> Observable prospects for Run 25 and  
<sup>438</sup> the EIC

<sup>439</sup> Chapter 16

<sup>440</sup> Remaining Questions

# <sup>441</sup> Chapter 17

<sup>442</sup> Implementation and application for  
<sup>443</sup> the remaining sPHENIX data

## <sup>444</sup> Bibliography

- <sup>445</sup> <sup>1</sup>R. Atkin, “Review of jet reconstruction algorithms”, Journal of Physics: Conference Series  
<sup>446</sup> **645**, 012008 (2015).
- <sup>447</sup> <sup>2</sup>G. P. Salam and G. Soyez, “A practical seedless infrared-safe cone jet algorithm”, Journal  
<sup>448</sup> of High Energy Physics **2007**, 086–086 (2007).
- <sup>449</sup> <sup>3</sup>Y. L. Dokshitzer, G. D. Leder, S. Moretti, and B. R. Webber, “Better jet clustering algo-  
<sup>450</sup> rithms”, JHEP 9708:001,1997 **1997**, 001–001 (1997).
- <sup>451</sup> <sup>4</sup>P. T. Komiske, E. M. Metodiev, and J. Thaler, “An operational definition of quark and  
<sup>452</sup> gluon jets”, JHEP 11 (2018) 059 **2018**, 10.1007/jhep11(2018)059 (2018).
- <sup>453</sup> <sup>5</sup>L. M. Jones, “Tests for determining the parton ancestor of a hadron jet”, Physical Review  
<sup>454</sup> D **39**, 2550–2560 (1989).
- <sup>455</sup> <sup>6</sup>Z. Fodor, “How to see the differences between quark and gluon jets”, Physical Review D  
<sup>456</sup> **41**, 1726–1730 (1990).
- <sup>457</sup> <sup>7</sup>J. Gallicchio and M. D. Schwartz, “Pure samples of quark and gluon jets at the lhc”,  
<sup>458</sup> Journal of High Energy Physics **2011**, 10.1007/jhep10(2011)103 (2011).
- <sup>459</sup> <sup>8</sup>D. Ferreira de Lima, P. Petrov, D. Soper, and M. Spannowsky, “Quark-gluon tagging with  
<sup>460</sup> shower deconstruction: unearthing dark matter and higgs couplings”, Physical Review D  
<sup>461</sup> **95**, 034001 (2017).
- <sup>462</sup> <sup>9</sup>B. Bhattacherjee, S. Mukhopadhyay, M. M. Nojiri, Y. Sakaki, and B. R. Webber, “Quark-  
<sup>463</sup> gluon discrimination in the search for gluino pair production at the lhc”, Journal of High  
<sup>464</sup> Energy Physics **2017**, 10.1007/jhep01(2017)044 (2017).
- <sup>465</sup> <sup>10</sup>P. Collaboration et al., “Creation of quark–gluon plasma droplets with three distinct ge-  
<sup>466</sup>ometries”, Nature Physics **15**, 214–220 (2019).
- <sup>467</sup> <sup>11</sup>sPHENIX Collaboration, “Sphenix technical design report”, May 2019.
- <sup>468</sup> <sup>12</sup>A. Adare et al., “An upgrade proposal from the phenix collaboration”, 10.48550/ARXIV.  
<sup>469</sup> **1501.06197** (2015).

- <sup>470</sup> <sup>13</sup>R. Belmont, J. Brewer, Q. Brodsky, P. Caucal, M. Connors, M. Djordjevic, R. Ehlers,  
<sup>471</sup> M. A. Escobedo, E. G. Ferreiro, G. Giacalone, Y. Hatta, J. Holguin, W. Ke, Z.-B. Kang,  
<sup>472</sup> A. Kumar, A. Mazeliauskas, Y. Mehtar-Tani, G. Nukazuka, D. Pablos, D. V. Perepelitsa,  
<sup>473</sup> K. Rajagopal, A. M. Sickles, M. Strickland, K. Tywoniuk, I. Vitev, X.-N. Wang, Z. Yang,  
<sup>474</sup> and F. Zhao, “Predictions for the sphenix physics program”, Nucl. Phys. A 1043 (2024)  
<sup>475</sup> 122821 **1043**, 122821 (2023).
- <sup>476</sup> <sup>14</sup>D. Lis and sPHENIX Collaboration, “Characterization of zero-suppression in sphenix  
<sup>477</sup> calorimeters and its impact on topological clusters”, in Aps division of nuclear physics  
<sup>478</sup> meeting abstracts, Vol. 2020, APS Meeting Abstracts (Jan. 2020), EN.007.
- <sup>479</sup> <sup>15</sup>C. Adler, A. Denisov, E. Garcia, M. Murray, H. Stroebele, and S. White, “The rhic zero  
<sup>480</sup> degree calorimeters”, Nuclear Instruments and Methods in Physics Research Section A:  
<sup>481</sup> Accelerators, Spectrometers, Detectors and Associated Equipment **470**, 488–499 (2001).
- <sup>482</sup> <sup>16</sup>A. J. Larkoski, G. P. Salam, and J. Thaler, “Energy correlation functions for jet substructure”,  
<sup>483</sup> Journal of High Energy Physics **2013**, 10.1007/jhep06(2013)108 (2013).